Clear-sky narrowband albedos derived from VIRS and MODIS

Sunny Sun-Mack[a], Patrick Minnis*[b], Yan Chen[a], and Robert F. Arduini[a]

[a]SAIC, 1 Enterprise Parkway, Suite 300, Hampton, VA USA 23666;
[b]Atmospheric Sciences, MS 420, NASA Langley Research Center, Hampton, VA USA 23681

ABSTRACT

The Clouds and Earth's Radiant Energy System (CERES) project is using multispectral imagers, the Visible Infrared Scanner (VIRS) on the Tropical Rainfall Measuring Mission (*TRMM*) satellite and the Moderate Resolution Imaging Spectroradiometer (MODIS) on *Terra*, operating since spring 2000, and *Aqua*, operating since summer 2002, to provide cloud and clear-sky properties at various wavelengths. This paper presents the preliminary results of an analysis of the CERES clear-sky reflectances to derive a set top-of-atmosphere clear sky albedo for 0.65, 0.86, 1.6, 2.13 µm, for all major surface types using the combined MODIS and VIRS datasets. The variability of snow albedo with surface type is examined using MODIS data. Snow albedo was found to depend on the vertical structure of the vegetation. At visible wavelengths, it is least for forested areas and greatest for smooth desert and tundra surfaces. At 1.6 and 2.1-µm, the snow albedos are relatively insensitive to the underlying surface because snow decreases the reflectance. Additional analyses using all of the MODIS results will provide albedo models that should be valuable for many remote sensing, simulation, and radiation budget studies.

Keywords: snow albedo, radiation, remote sensing, spectral albedo, MODIS, CERES, VIRS

1. INTRODUCTION

One of the critical parameters for detecting clouds and aerosols and for deriving their microphysical properties is the clear-sky radiance. Knowledge of the spatial and angular variability of clear-sky albedo is an essential first step for predicting the clear-sky radiance at solar wavelengths. Three spectra used in the detection and classification of clouds for the Clouds and the Earth's Radiant Energy System (CERES) Experiment are the visible (VIS; 0.65 µm) and near-infrared (NIR; 1.6, 2,13 µm) channels on the imagers used by CERES[1]. Another channel sometimes used for cloud detection, aerosol retrievals, and vegetation cover assessment is the vegetation (VEG; 0.86-µm) channel that has been available, along with the VIS channel, on the Advanced Very High Resolution Radiometer (AVHRR) for many years. Generally, clear-sky albedo for a given surface type is determined for conditions when the vegetation is either thriving or dormant without snow cover. Snow albedos are usually determined without regard to the underlying surface type. However, the albedo for a given surface that is blanketed by snow should vary with the surface type because of tendencies for vegetation to emerge from the snow to various degrees depending on the vertical dimensions of the vegetation. For example, a snow-covered forest will tend to be darker than a snow-covered prairie because the snow will eventually fall off the trees exposing the darker surfaces while the snow on a grassland at the same temperatures will likely be continuous and, therefore, more reflective. Accounting for these vegetation-type differences should improve the capabilities for distinguishing snow and clouds for different surface types and facilitate improvements in the accuracy of radiative transfer calculations between the snow-covered surface and the atmosphere, eventually leading to improvements n the modeling of snow processes over land.

This paper examines the variations in clear-sky albedos for both snow-free and snow-covered surfaces for four spectral channels using data from the Moderate Resolution Imaging Spectroradiometer (MODIS) on *Aqua*. The first imager used by CERES is the Visible Infrared Scanner (VIRS) on the Tropical Rainfall Measuring Mission (*TRMM*) satellite. Because of TRMM's 35°-inclined-orbit, the VIRS takes measurements at all times of day over a given region between 37°N and 37°S during a period of 46 days. Thus, the VIRS data provided the opportunity to derive albedo values over all solar zenith angles (SZA)[2] and, despite some spectral differences with the corresponding MODIS channels, give a

---

* p.minnis@nasa.gov; phone 1 757 864-5671; fax 1 757 864-7996; www-pm.larc.nasa.gov

baseline snow-free albedo dataset. Later, clear-sky albedos were derived from measurements by MODIS on the sun-synchronous *Terra*, which had a 1030 Local Time (LT) equatorial crossing. Because of the *Terra* orbit, it is not possible to derive the albedos for all SZAs and the SZA dependence is different from that for VIRS for, at least, the MODIS VIS channel because of greater Rayleigh scattering in the VIRS bandwidth[3]. Comparisons of albedos must account for the SZA dependence over a given scene type, so the Rayleigh scattering component should be adjusted for any bandwidth differences. *Aqua* is in a 1330-LT sun-synchronous orbit, so the SZA range for a given location should be the similar for both *Terra* and *Aqua* and for portions of the *TRMM* VIRS data. The albedos derived from VIRS, *Terra*, and *Aqua* are used to compare with the preliminary values from Aqua for snow-covered land.

2. DATA & METHODOLOGY

Aqua began producing MODIS imagery in early summer 2002. Except for the 1.6-µm channel, the *Aqua* MODIS sensors appeared to be working well. For CERES, every other 1-km MODIS pixel and scan line was skipped to achieve an effective 2-km resolution to minimize processing time and data storage. Each MODIS pixel is initially classified as clear or cloudy using updated versions of the CERES classification schemes[4-5] that rely on the radiances measured by the VIS, NIR, 3.7-µm, 11-µm, and 12-µm channels. The radiances are compared with predicted clear-sky radiances based on empirical estimates of spectral clear-sky albedo[2-3] and on skin temperatures from the European Center for Medium-range Weather Forecasting (ECMWF) reanalyses adjusted using empirical estimates of spectral surface emissivity[6-7] and atmospheric absorption calculated with the ECMWF vertical profiles of temperature and humidity.

All clear pixels for a given overpass are averaged into the appropriate region defined by a 10' global grid. Each 10' region is assigned a single surface type K as defined by the International Geosphere Biosphere Programme (IGBP). The mean observed clear-sky reflectance for the overpass is

$$\rho_\lambda = \rho_\lambda(K; LAT, LON; \mu_o, \mu, \psi) \qquad (1)$$

where λ is the wavelength, K is the International Geosphere Biosphere Programme (IGBP) surface type (see Table 1), LAT and LON are the latitude and longitude, respectively, μ_o and μ are the cosines of SZA and viewing zenith angle (VZA), respectively, and ψ is the relative azimuth angle. Instantaneous regional mean or pixel-level clear-sky reflectances comprise the fundamental data used here.

Clear-sky reflectance is a combination of radiation reflected by the atmosphere and the surface. For the VIS (0.65-µm) channels, the primary atmospheric effects are Rayleigh and aerosol scattering and ozone absorption, while water vapor absorption and aerosols are the primary attenuators in the NIR channels. The effects of water vapor and aerosols are generally minor except for aerosols over ocean. Calibration studies show that the VIRS VIS reflectance is up to 0.02 greater than MODIS at low values that can be explained mostly by the Rayleigh scattering differences[4].

To account for the anisotropy of the reflected radiation, each reflectance is converted to albedo,

$$\alpha_\lambda = \rho_\lambda (K; LAT, LON; \mu_o, \mu, \psi) / \chi_\lambda(K; \mu_o, \mu, \psi), \qquad (2)$$

where χ_λ is the normalized bidirectional reflectance distribution function (BRDF) for the particular surface type and wavelength. For all wavelengths over water surfaces, the BRDF values are taken from an empirical model based on geostationary satellite data[8]. An empirical model[9] is also used for all wavelengths over barren desert scenes. The snow BRDFs[10-11] for each were developed from calculations using an adding-doubling radiative transfer model. The snow surface was approximated using a layer made up of randomly oriented, hexagonal ice crystals having a length to width ratio L/D of 750µm/160µm[12] with an optical depth of 1000. The model BRDFs at the top of the atmosphere were computed using a radiative transfer model incorporating the May 22 (clear-sky) Arctic atmosphere from the European Center for Medium-Range Weather Forecasting analysis and a correlated k-distribution method[13]. The snow BRDFs were used for permanent ice/snow surfaces and for any other scene classified as snow covered. For $K = 19$, an empirical coastal model[9] was used for all wavelengths. The empirical land model[9] was used for the VIS channel over all remaining surface types ($K = 1-14, 18$) .The BRDFs for the other channels and remaining surface types

Table 1: Surface type categories and overhead sun albedos from VIRS and MODIS.

K	IGBP Type	VIRS α_o		MODIS α_o			Snow Type
		0.65 µm	1.64 µm	0.64 µm	0.87 µm	1.62 µm	2.13 µm	
1	evergreen needleleaf	0.091	0.166	0.087	0.175	0.182	0.093	forest
2	evergreen broadleaf	0.099	0.146	0.097	0.206	0.174	0.070	forest
3	deciduous needleleaf	0.096	-------	0.108	-------	0.196	0.117	forest
4	deciduous broadleaf	0.100	0.177	0.099	0.189	0.216	0.113	forest
5	mixed forest	0.098	0.158	0.097	0.184	0.198	0.094	forest
6	closed shrubland	0.135	0.150	0.126	0.185	0.195	0.072	grass
7	open shrubland	0.172	0.325	0.177	0.206	0.368	0.222	grass
8	woody savanna	0.112	0.110	0.120	0.173	0.136	0.059	grass
9	savanna	0.120	0.246	0.118	0.191	0.292	0.179	grass
10	grassland	0.145	0.286	0.142	0.207	0.319	0.228	grass
11	permanent wetland	0.079	0.200	0.082	0.116	0.222	0.123	coast
12	cropland	0.125	0.236	0.119	0.181	0.257	0.150	grass
13	urban	0.121	0.202	0.102	0.186	0.229	0.121	grass
14	mixed grass-forest	0.106	0.210	0.112	0.185	0.271	0.151	grass
15	snow-ice	0.589	0.218	0.475	0.855	0.150	0.144	snow-ice
16	desert, barren/sparse vegetation	0.296	0.455	0.304	0.321	0.525	0.407	desert
17	water	0.062	0.022	0.072	0.044	0.031	0.022	water
18	tundra	0.238	0.177	0.249	0.166	0.200	0.163	desert
19	coastline (10-90% water)	0.090	0.129	0.067	0.150	0.135	0.099	coast

were derived from aircraft measurements[14] taken at 0.877, 1.66, and 2.13 µm for four distinct surfaces. The coniferous forest models were used for all forest types ($K = 1,5$), while bog was used for $K = 11, 18$, and 19. The savanna data were used for $K = 6, 7, 8, 9$, and 13 and the pasture results were used for $K = 10, 12$, and 14.

The resulting top-of-atmosphere (TOA) albedos for each pixel were then averaged for every 0.1 interval of μ_o to examine the SZA dependence. The means for the 19 IGBP types were further averaged into 6 snow types based on vegetation or amount of water surface as listed in Table 1. At the time of this writing, the analyses had been completed for only 1 month of *Aqua* data, September 2002, and for 3 days of *Terra* MODIS data taken during January 2003. Thus, the results presented here are considered preliminary since the primary regions with potential for snow cover in the Northern Hemisphere are mostly snow free during September. The mean TOA overhead-sun albedos α_o were computed from the SZA-binned albedos using a set of empirical directional reflectance models (DRMs) from VIRS for 0.65 and 1.6-µm data[2]. The former and latter DRMs were used also for 0.87 and 2.1 µm, respectively. The results are listed in Table 1 for snow-free conditions using VIRS VIS data from September 2000 and 1.6-µm data from January 1998. September 2002 *Aqua* MODIS clear-sky data were used for 0.64 and 2.13-µm data, while *Terra* MODIS data from September 2002 were used for the 0.87 and 1.62-µm albedos. The VIRS 1.6-µm albedos are approximately 20% lees than their MODIS counterparts suggesting some calibration differences between the two sensors. The VIRS and *Aqua* MODIS VIS albedos are very comparable.

3. RESULTS AND DISCUSSION

Figure 1 shows the distribution albedos for snow-free and snow-covered areas during September 2003. Most of the snow-covered areas are confined to latitudes poleward of 60° with the exception of a few areas like the Tibetan Plateau, the Andes, and the Canadian Rocky Mountains. Areas along the edge of the girdle of sea ice around Antarctica show the beginnings of summer melting while coastal areas around the Arctic Ocean are beginning to freeze. The mean albedos for September and January for permanent snow-ice, IGBP category 15, are plotted in Fig. 2 to provide a reference point for the snow albedos over other surface types. Both datasets show much lower albedos at small SZAs (large μ_o) for the VIS and VEG channels compared to the values for $\mu_o < 0.7$ (Fig. 2a). The higher VIS values are consistent with those from theoretical calculations that indicate reflectances varying between 0.82 and 0.88 for pure snow surfaces[5]. The lower values at large μ_o are probably mostly from midlatitude and subtropical glaciers that may be less continuous than
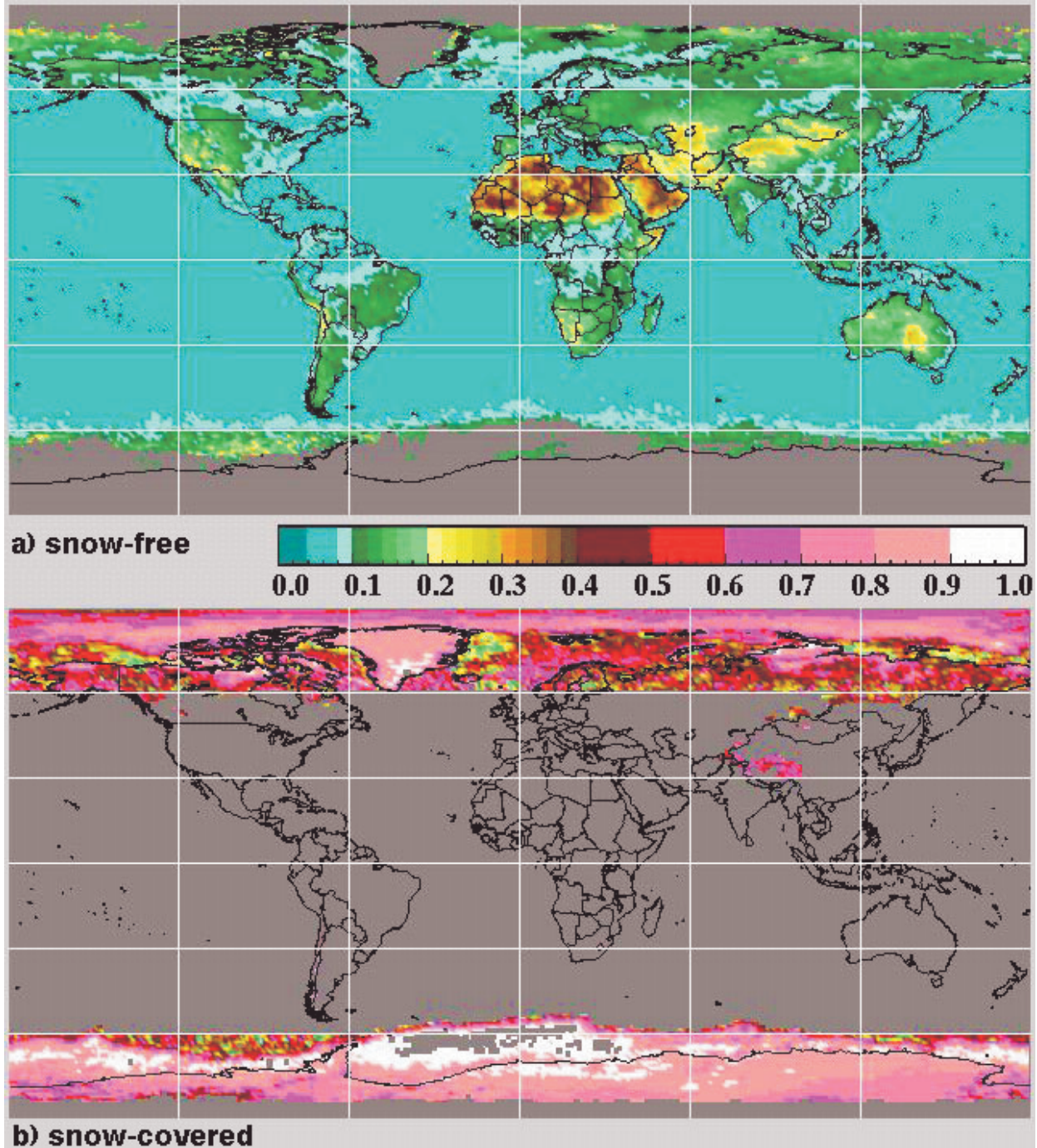
Figure 1: Mean TOA clear-sky VIS (0.65 µm) albedos from *Aqua* MODIS data during September 2002.

polar snowfields and may be dirtier than their polar counterparts. Additionally, at the small SZAs, more surface melting may occur causing a reduction in the albedo. The NIR albedos (Fig. 2b) are considerably lower due to the strong absorption by the large snow crystals. The *Aqua* albedos tend to increase with increasing SZA while the changes in the *Terra* albedos with SZA are generally much smaller. Good agreement for *Terra* and *Aqua* in both the 1.6 and 2.1-µm albedos is evident for $\mu_o > 0.4$. The albedos diverge at larger SZAs, perhaps because of differences in the sampled fields between the two months. In general, it appears that for pure snow surfaces, the mean 1.6 and 2.1-µm albedos are roughly 0.10 and 0.05, respectively. The VIS and VEG albedos are around 0.85 except for the high-sun cases.
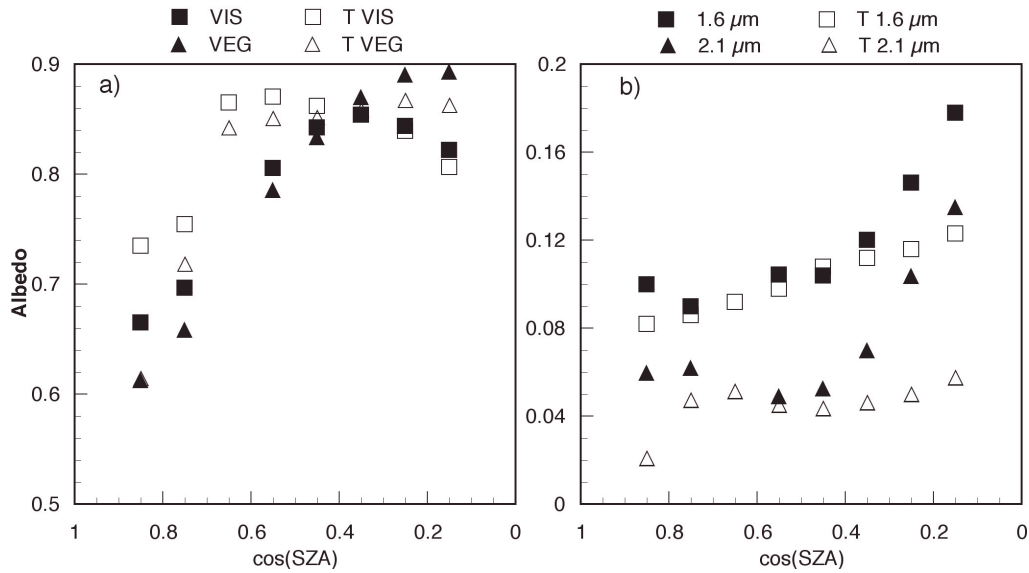
Figure 2: Mean spectral albedos for permanent snow-ice surfaces from September 2002 *Aqua* and January 2003 *Terra* (denoted with "T") MODIS data.

Figure 3 shows the albedos over forested land derived from the September 2002 *Aqua* MODIS data. For snow-free conditions, the VIS albedo increases with SZA while the VEG albedo decreases (Fig. 3a). This latter variation is most likely due to the latitudinal changes in broadleaf deciduous trees that begin to lose chlorophyllic leaf mass during September in the northern mid-latitudes. Most of the albedos for $\mu_o > 0.6$ are from midlatitude forests. The VIS channel is much less sensitive to vegetation changes. The VIS and VEG albedos increase substantially over forests when they are blanketed with snow. The VIS values average around 0.50, while the VEG albedos range from 0.48 to 0.65 depending on the mean albedo of the snow-free background. These snow-scene albedos are 40% less than those for the permanent snow-ice areas. The opposite behavior occurs for the NIR channels with the snow-free albedos exceeding their counterparts with snow.

Over grass and shrub lands (Fig. 4), all of the spectral albedos are greater than those over forests. Both the VEG and VIS albedos tend to increase with SZA for snow-free conditions. The mean VIS and VEG albedos in snow-covered
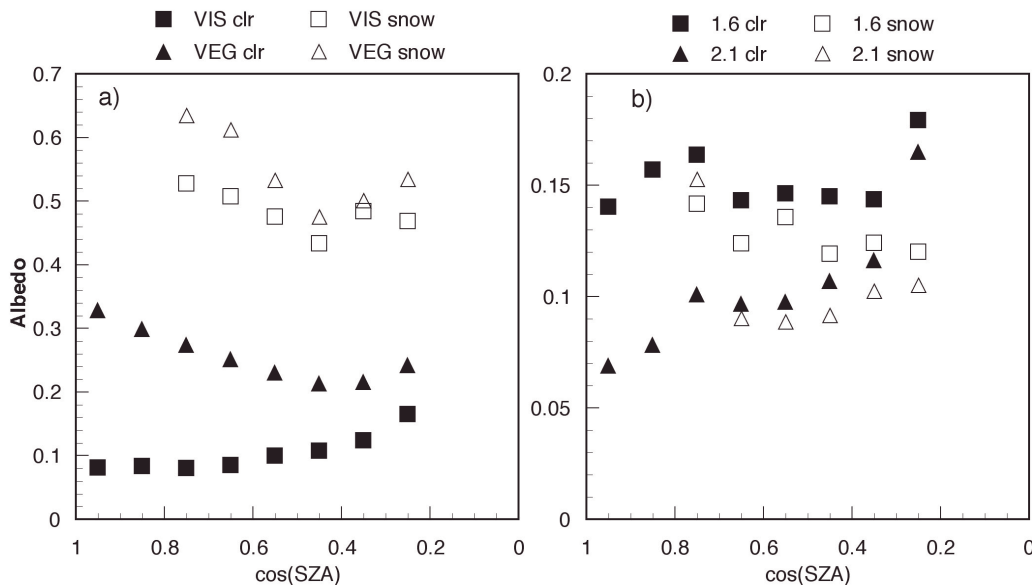

Figure 3: Spectral albedos derived over forests from *Aqua* data for snow-free (clr) and snow-covered (snow) conditions.
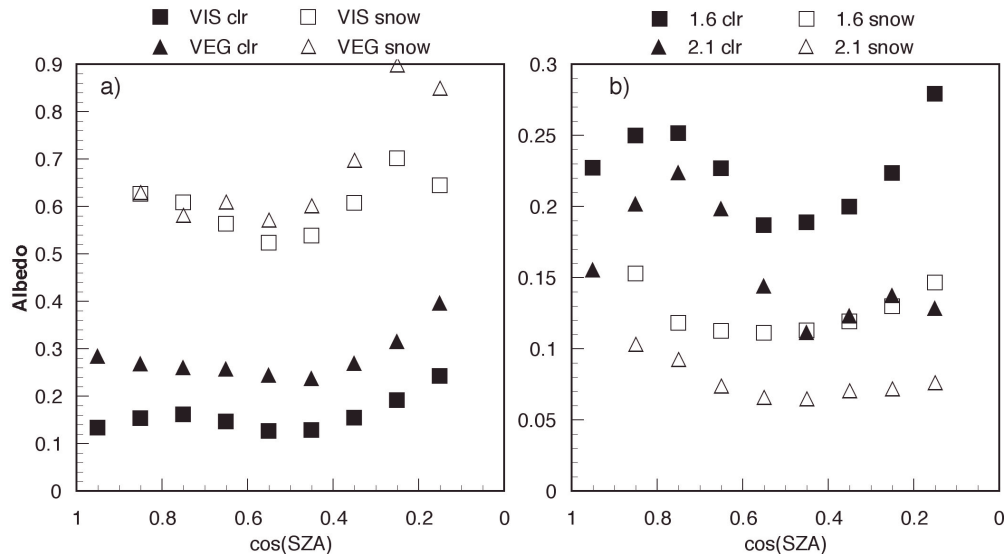
Figure 4: Spectral albedos derived over grass and shrub lands from *Aqua* data for snow-free (clr) and snow-covered (snow) conditions.

conditions are roughly 0.60 and 0.68, respectively (Fig. 4a). The NIR snow-free albedos over grass are nearly double the values for their snow-covered counterparts (Fig. 4b). The variations with SZA for all of the snow albedos in Fig. 4 are probably influenced by the greater insolation and by increased vegetation contamination at greater values of μ_o. In desert and tundra areas, the VEG and VIS albedos are much closer than over the other vegetated areas (Fig. 5a). For snow-free conditions, the VEG, VIS, and NIR (Fig. 5b) albedos all decrease dramatically between $\mu_o = 1$ and 0.6 and remain relatively constant at smaller values of μ_o. This dependence is due to the changing nature of the scenes with latitude. At low latitudes (large μ_o), the very bright deserts in North Africa and the Arabian Peninsula dominate the averages (Fig. 1), while at higher latitudes, darker deserts and slightly vegetated tundra prevail. Despite the great variations in background albedos when no snow is present, the albedos are relatively flat with SZA when snow is present. The VIS albedo changes smoothly from ~0.67 at $\mu_o = 0.85$ to 0.84 at $\mu_o = 0.25$. The VEG albedo varies even less. Over ocean, the albedos appear to behave more predictably than over land surface due to a combination of greater sampling and surface homogeneity than over land. Compared to land areas, the albedos over the temporarily snow and ice-covered waters (Fig. 6) are much closer to those for the permanent snow-ice areas except at the higher values of μ_o. At $\mu_o = 0.55$, the VEG and VIS albedos (Fig. 6a) are lower due to melt ponds and to pixels only partially covered with
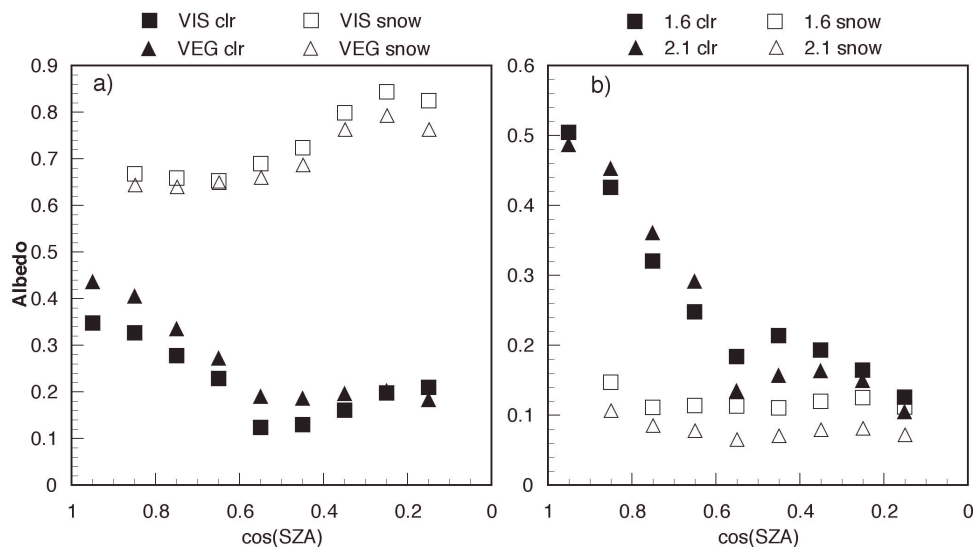

Figure 5: Spectral albedos derived over desert and tundra from *Aqua* data for snow-free (clr) and snow-covered (snow) conditions.
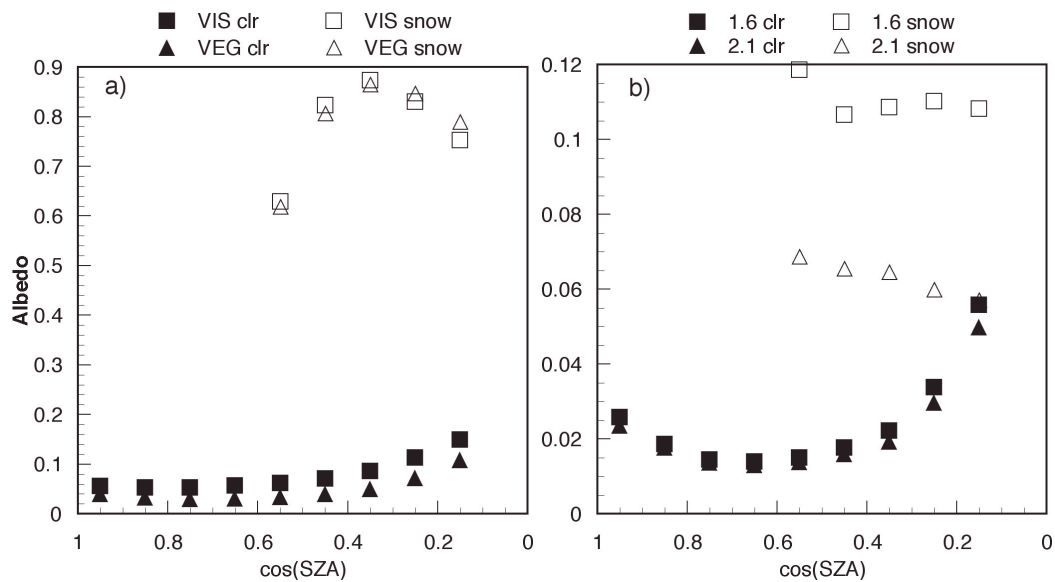
Figure 6: Spectral albedos derived over water surfaces from *Aqua* data for snow-free (clr) and snow-covered (snow) conditions.

ice (e.g., floes or icebergs). Unlike the land areas, snow raises the NIR albedos over ocean by factors of 4 or 5 (Fig. 6b). The albedos over coastal areas are between those over ocean and land (not shown).

Understanding the differences in the albedos for various surface types requires requires comparisons at the same SZA. When the DRM is known for each surface types, it is possible to determine α_o and have a basis for comparison (e.g., Table 1). However, such DRMs are not currently available for the different land surfaces covered by snow. The latitudinally dependent SZA sampling by single sun-synchronous satellites, for the most part, precludes their derivation. To overcome these sampling difficulties, the mean albedos are computed for each category using the μ_o-weighted values for μ_o between 0.55 and 0.25, the angles where all of the categories have values. The mean μ_o corresponds to SZA = 66.4°. The resulting mean values are summarized in Table 2. The maximum land snow-free albedos are found for the VEG channel while the minimum values occur at 2.1 µm. The ocean albedo is greatest at 0.65 µm and least at 2.1 µm. When snow covers the various surfaces, the VIS and VEG albedos increase according to the vertical structure of the vegetation. The values over land are least for the forest and greatest for smoother desert and tundra surfaces with grass-shrub vegetation in the middle. Once snow collects on an ice covered ocean surface, however, the VIS/VEG albedos exceed those over land and are closest to the those for areas permanently covered by snow and ice. However, some of the areas that are classified as permanent snow-ice actually undergo melting exposing the underlying surfaces. These surfaces are generally dark and probably consist of ocean and rock. Thus, all of the snow-free albedos are between those for ocean and coastline. The *Aqua* VIS/VEG albedos for the permanent snow-ice locations are slightly less than those from *Terra* suggesting either some slight calibration differences or a greater abundance of pure snow

Table 2: Mean albedos at SZA = 66.4° from September 2002 *Aqua* MODIS and January 2003 *Terra* MODIS data (denoted by "T").

Snow category	snow -free				snow-covered			
	0.65 µm	0.87 µm	1.6 µm	2.1 µm	0.65 µm	0.87 µm	1.6 µm	2.1 µm
forest	0.118	0.225	0.150	0.115	0.465	0.510	0.126	0.095
grass	0.144	0.259	0.196	0.129	0.574	0.658	0.116	0.067
desert	0.145	0.192	0.191	0.150	0.747	0.710	0.115	0.072
coast	0.122	0.171	0.127	0.091	0.547	0.531	0.116	0.071
ocean	0.078	0.045	0.020	0.018	0.769	0.760	0.112	0.065
snow-ice	0.101	0.093	0.073	0.061	0.833	0.834	0.114	0.063
snow-ice (T)	N/A				0.860	0.855	0.107	0.045

during January 2003. The mean NIR albedos for the snow-covered surfaces are remarkably invariant with surface type, especially at 1.6 µm. This behavior was implicit in the development of the snow detection algorithm, which relies heavily on the reflectance at 3.7 µm[11], but was never tested. It is likely that the 3.7-µm albedos behave in a similar manner. The *Aqua* NIR albedos for permanent snow and ice are less than those from *Terra*, again reflecting the possible sampling or calibration differences. Over the land areas, the 2.1-µm snow albedos are about 25% greater than the permanent snow-ice value indicating some influence of the vegetation on the albedo.

4. CONCLUSIONS

The preliminary results shown here demonstrate the variability of snow albedo with surface type for spectral channels commonly used for Earth and atmospheric remote sensing. The vertical structure of vegetation has a significant influence on the snow albedos and should be taken into account for both remote sensing and radiation budget purposes. It is clear that the combinations of the various channels can be refined to further improve the discrimination between scenes with clouds and those with snow on the surface. Future studies will take advantage of the large clear and cloudy database already developed by CERES from the *TRMM*, *Terra*, and *Aqua* imager datasets[15]. Those datasets, after proper intercalibrations, should improve the statistics, including standard deviations, for all of the surface types and solar zenith angles. Because the spectral albedos vary for the IGBP types within the "snow categories" used here, albedo statistics should also be derived for each individual IGBP type.

ACKNOWLEDGMENTS

REFERENCES

1. Wielicki, B. A., et al., 1998, Clouds and the Earth's Radiant Energy System (CERES): Algorithm overview. *IEEE Trans. Geosci. Remote Sens.*, **36**, 1127-1141.
2. Sun-Mack, S., Y. Chen, T. D. Murray, P. Minnis, and D. F. Young, Visible clear-sky and near-infrared surface albedos derived from VIRS for CERES. *Proc. AMS 10th Conf. Atmos. Rad.*, Madison, WI, June 28–July 2, 422-425, 1999.
3. Chen, Y., S. Sun-Mack, Q. Z. Trepte, P. Minnis, and D. F. Young, Solar zenith angle variation of clear-sky narrowband albedos derived from VIRS and MODIS. *Proc. 11th AMS Conf. Atmos. Rad.*, Ogden, UT, June 3-7, 152-155, 2002.
4. Trepte, Q., Y. Chen, S. Sun-Mack, P. Minnis, D. F. Young, B. A. Baum, and P. W. Heck, Scene identification for the CERES cloud analysis subsystem. *Proc. AMS 10th Conf. Atmos. Rad.*, Madison, WI, June 28 – July 2, 169-172, 1999.
5. Trepte, Q. Z., P. Minnis, and R. F. Arduini, Daytime and nighttime polar cloud and snow identification using MODIS. *Proc. SPIE Conf. Optical Remote Sensing of Atmosphere and Clouds III*, Hangzhou, China, Oct. 23-27, 2002.
6. Chen, Y., S. Sun-Mack, P. Minnis, W. L. Smith, Jr., and D. F. Young, Surface emissivity derived for infrared remote sensing from satellites. *Proc. AMS 11th Conf. Satellite Meteorology and Oceanography.*, Madison, WI, October 15-18, 512-515, 2001.
7. Chen, Y., S. Sun-Mack, Surface spectral emissivity derived from MODIS data. *Proc. SPIE Conf. Optical Remote Sensing of Atmosphere and Clouds III*, Hangzhou, China, Oct. 23-27, 2002.
8. Minnis, P. and E. F. Harrison, Diurnal variability of regional cloud and clear-sky radiative parameters derived from GOES data. Part III: November 1978 radiative parameters. *J. Climate Appl. Meteor.*, **23**, 1032-1051, 1984.
9. Suttles, J. T., R. N. Green, P. Minnis, G. L. Smith, W. F. Staylor, B. A. Wielicki, I. Walker, D. F. Young, V. R. Taylor, and L. L. Stowe, Angular radiation models for Earth-atmosphere system, Vol. 1, Shortwave radiation. *NASA RP-1184*, 144 pp, 1988.
10. Trepte, Q., R. F. Arduini, Y. Chen, S. Sun-Mack, P. Minnis, D. A. Spangenberg, and D. R. Doelling, Development of a daytime polar cloud mask using theoretical models of near-infrared bidirectional reflectance For ARM and CERES. *Proc. AMS 6th Conf. on Polar Meteorology and Oceanography*, San Diego, CA, May 14-18, 242-245, 2001.

11. Spangenberg, D. A., V. Chakrapani, D. R. Doelling, P. Minnis, and R. F. Arduini, Evaluation of an automated Arctic cloud mask using observations from SHEBA and the ARM North Slope of Alaska Site. *Proc. AMS 6th Conf. Polar Meteorology and Oceanography*, San Diego, CA, May 14-18, 246-249, 2001.
12. Takano, Y. and K. N. Liou, Radiative transfer in cirrus clouds: I single scattering and optical properties of oriented hexagonal ice crystals. *J. Atmos. Sci.*, **46**, 3-20, 1989.
13. Kratz, D.P., The correlated-k distribution technique as applied to the AVHRR channels. *J. Quant. Spectrosc. Radiat. Transfer*, **53**, 501-51, 1995.
14. Kriebel, K. T., Measured spectral bidirectional reflectance properties of vegetated surfaces. *Appl. Opt.*, **17**, 253-259, 1978.
15. Minnis, P., D. F. Young, S. Sun-Mack, and P. W. Heck, CERES cloud property retrievals from imagers on TRMM, Terra, and Aqua. *Proc. SPIE Conf. Remote Sensing of Clouds and the Atmosphere VII*, Barcelona, Spain, Sept. 8-12, 2003.